Cell Reports

Metabolic Reprogramming of Pancreatic Cancer Mediated by CDK4/6 Inhibition Elicits Unique Vulnerabilities

Graphical Abstract

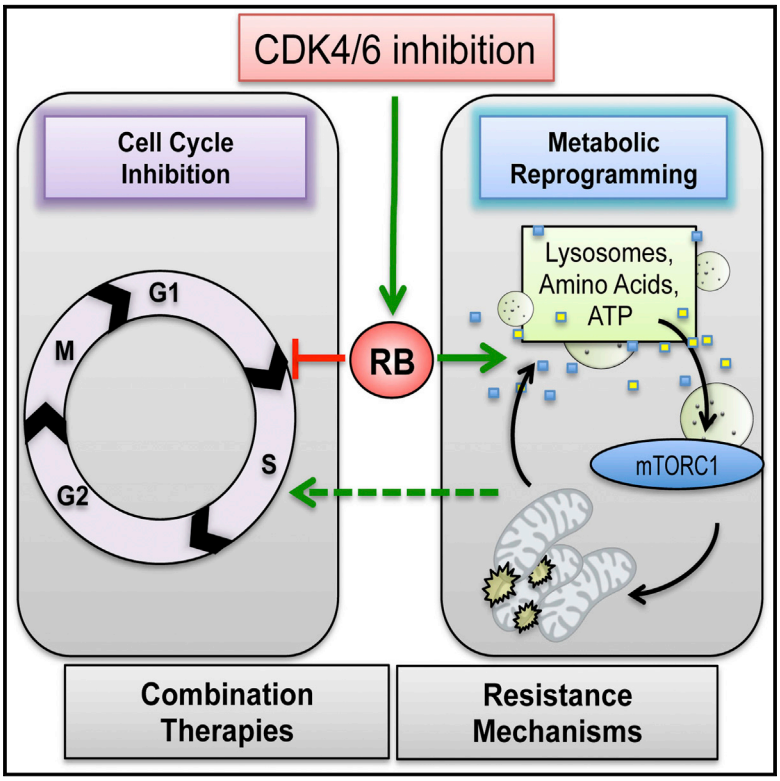

Highlights

- CDK4/6 inhibition increases oxidative phosphorylation through the RB pathway
- Compensatory activation of MTOR occurs downstream of CDK4/6 inhibition
- Combination treatments have disparate effects on cellular metabolism
- Therapeutically targeting select features of CDK4/6 arrested cells is feasible

Authors

Jorge Franco, Uthra Balaji, Elizaveta Freinkman, Agnieszka K. Witkiewicz, Erik S. Knudsen

Correspondence

agnes.witkiewicz@utsouthwestern.edu (A.K.W.), erik.knudsen@utsouthwestern.edu (E.S.K.)

In Brief

CDK4/6 inhibitors are potent inhibitors of cell cycle that are employed clinically. Franco et al. report that the inhibition of CDK4/6 in pancreatic cancer models reprograms metabolism through a pathway involving the RB tumor suppressor and MTOR activation. These findings demonstrate specific metabolic adaptations to this class of therapeutic agents and delineate vulnerabilities for future therapeutic intervention.

Franco et al., 2016, Cell Reports *14*, 979–990
February 9, 2016
http://dx.doi.org/10.1016/j.celrep.2015.12.094

Cell Reports
Report

Metabolic Reprogramming of Pancreatic Cancer Mediated by CDK4/6 Inhibition Elicits Unique Vulnerabilities

Jorge Franco,[1] Uthra Balaji,[1] Elizaveta Freinkman,[3] Agnieszka K. Witkiewicz,[1,2,*] and Erik S. Knudsen[1,2,*]
[1]McDermott Center University of Texas Southwestern Medical Center, 6000 Harry Hines Boulevard, Dallas, TX 75390, USA
[2]Simmons Cancer Center, University of Texas Southwestern Medical Center, 6000 Harry Hines Boulevard, Dallas, TX 75390, USA
[3]Whitehead Institute, Massachusetts Institute of Technology, 9 Cambridge Center, Cambridge, MA 02142, USA
*Correspondence: agnes.witkiewicz@utsouthwestern.edu (A.K.W.), erik.knudsen@utsouthwestern.edu (E.S.K.)
http://dx.doi.org/10.1016/j.celrep.2015.12.094

SUMMARY

Due to loss of p16ink4a in pancreatic ductal adenocarcinoma (PDA), pharmacological suppression of CDK4/6 could represent a potent target for treatment. In PDA models, CDK4/6 inhibition had a variable effect on cell cycle but yielded accumulation of ATP and mitochondria. Pharmacological CDK4/6 inhibitors induce cyclin D1 protein levels; however, RB activation was required and sufficient for mitochondrial accumulation. CDK4/6 inhibition stimulated glycolytic and oxidative metabolism and was associated with an increase in mTORC1 activity. MTOR and MEK inhibitors potently cooperate with CDK4/6 inhibition in eliciting cell-cycle exit. However, MTOR inhibition fully suppressed metabolism and yielded apoptosis and suppression of tumor growth in xenograft models. The metabolic state mediated by CDK4/6 inhibition increases mitochondrial number and reactive oxygen species (ROS). Concordantly, the suppression of ROS scavenging or BCL2 antagonists cooperated with CDK4/6 inhibition. Together, these data define the impact of therapeutics on PDA metabolism and provide strategies for converting cytostatic response to tumor cell killing.

INTRODUCTION

Pancreatic ductal adenocarcinoma (PDA) has a 5-year survival of only ~6% (Saif, 2013; Vincent et al., 2011). This dire prognosis is due to multiple clinical features of the disease, including diagnosis at late stage and ineffective systemic therapies (Paulson et al., 2013). Therefore, there is significant energy directed at delineating biological features of PDA that could be exploited for therapeutic intervention.

One of the hallmark genetic events in PDA is loss of the CDKN2A/2B tumor suppressor locus (Maitra and Hruban, 2008). This locus encodes endogenous CDK4/6 inhibitors that are particularly relevant in the context of KRAS-driven tumors, such as PDA (LaPak and Burd, 2014; Witkiewicz et al., 2011). Oncogenic KRAS can induce a senescent-like growth arrest state in cells (Serrano et al., 1995, 1997). The execution of this phenotype is mediated by p16ink4a encoded by CDKN2A that blocks the activity of CDK4/Cyclin D and CDK6/Cyclin D complexes (Serrano et al., 1995; Witkiewicz et al., 2011). This leads to the suppression of RB phosphorylation and concomitant inhibition of cell-cycle progression through the suppression of E2F-mediated transcription (Chicas et al., 2010). Highly selective drugs that phenocopy features of p16ink4a function would be expected to have potency in PDA (Asghar et al., 2015). While such drugs have some degree of effect in established PDA cell lines (Franco et al., 2014; Heilmann et al., 2014; Liu and Korc, 2012; Witkiewicz et al., 2015a), resistance can develop quickly, thereby necessitating the use of combination therapeutic approaches.

Although the underlying mechanisms remain unclear, cell division is coordinated with metabolic functions. First observed in yeast, cell-cycle entry is associated with increased cellular mass and the accumulation of energetic metabolites required for cell division (Cai and Tu, 2012). In PDA, much of the metabolic circuitry is subservient to mutant KRAS, which drives a complex reprogramming of glycolytic, oxidative and non-canonical (e.g., macropinocytosis) metabolic pathways in concert with tumorigenic proliferation (Bryant et al., 2014; Sousa and Kimmelman, 2014). Key downstream effectors include MEK and MTOR signaling pathways that engage multiple distal features of metabolism through transcriptional and translational regulatory programs (Laplante and Sabatini, 2009, 2012; Viale et al., 2014; Ying et al., 2012). The interface of cell-cycle regulatory factors with metabolism is similarly complex and varied (Lopez-Mejia and Fajas, 2015). For example, Cyclin D1, which is a requisite activator of CDK4/6, has been shown to act in a transcriptional role to coordinate metabolism and mitochondrial function (Wang et al., 2006). Additionally, at a cellular and organismal level CDK4/6 activity plays important roles in controlling gluconeogenesis and responsiveness to insulin (Lopez-Mejia and Fajas, 2015). RB has been shown to bind to mitochondria and regulate apoptotic functions (Hilgendorf et al., 2013), while E2F has been shown to drive mitochondrial-dependent apoptosis in *Drosophila* (Ambrus et al., 2013; Benevolenskaya and Frolov, 2015). Interestingly, in fibroblastic models RB loss is associated

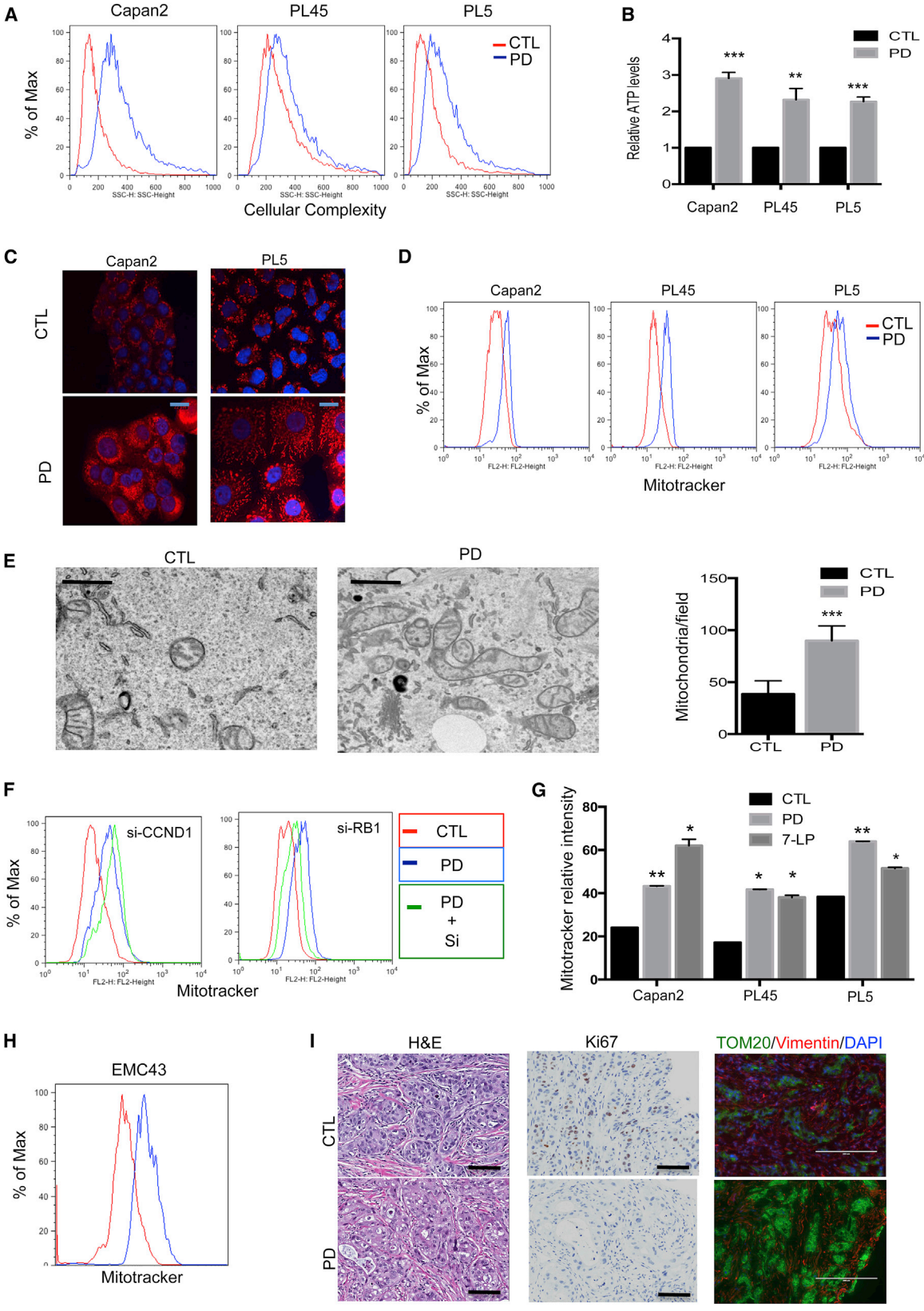

(legend on next page)

with increased glutamine utilization (Clem and Chesney, 2012; Reynolds et al., 2014), and loss of RBF has been associated with altered glutamine catabolism in *Drosophila* (Nicolay et al., 2013). Recent studies have shown that loss of RB can lead to decreased oxidative phosphorylation and more dependency on glycolytic metabolism (Nicolay et al., 2015; Váraljai et al., 2015). Consonantly, E2F1 and RB in tissue can provide a critical node of regulation between proliferation and metabolic activity (Blanchet et al., 2011; Lopez-Mejia and Fajas, 2015). Since metabolic features of cancer are progressively emerging as a target for therapeutic intervention, these findings supported a direct interrogation of how pharmaceutical CDK4/6 inhibitors impinge on tumor metabolism and the ability to selectively target that metabolic state.

RESULTS

CDK4/6 Inhibition Yields Increased Mitochondrial Mass via RB

In order to address the role of CDK4/6 inhibition in PDA, three cell models were utilized. These models contain classic genetic features of PDA (Franco et al., 2014) but exhibit differing cell-cycle inhibition with pharmacological suppression of CDK4/6 activity (Figure S1). While many therapeutic agents that target KRAS signaling suppress metabolism, we observed that CDK4/6 inhibition with PD-0332991 resulted in increased cellular complexity, which is an indirect surrogate of increased organelles and metabolic functions within the cytoplasm (Figure 1A). Concordantly, CDK4/6 inhibition was accompanied by an increase in ATP levels (Figure 1B) and an increase in mitochondrial mass in multiple cell lines (Figures 1C and 1D; Figure S1). Because these effects could represent a specific feature of PD-0332991 as opposed to CDK4/6 inhibition, two other specific CDK4/6 inhibitors (LEE-11 and LY2853219) were employed and exhibited similar increased MitoTracker staining (Figure S1). Transmission electron microscopy confirmed the numerical increase in mitochondria in cells treated with CDK4/6 inhibitors (Figure 1E).

CDK4/6 inhibitors are known to inhibit cell cycle (Asghar et al., 2015) but also exert two biochemical effects that are potentially germane to tumor metabolism. Notably, CDK4/6 inhibitors will lead to the accumulation of Cyclin D1, which has the capacity to impact cell biology through non-catalytic functions (Lamb et al., 2003), and CDK4/6 inhibition results in the suppression of RB phosphorylation (Dean et al., 2010; Fry et al., 2004) (Figure S1). Using RNAi-mediated knockdown (Figure S1), Cyclin D1 depletion had little effect on mitochondrial accumulation (Figure 1F). In contrast, the knockdown of RB1 partially reverted the accumulation of mitochondria (Figure 1F) and decreased cellular complexity (Figure S1). Additionally, we defined rare cases of PDA that exhibit endogenous RB loss (Witkiewicz et al., 2015b). Using a cell line derived from such a case (EMC7310), we observed that the increase in mitochondrial mass was dependent on RB (Figure S1). Furthermore, employing a constitutively active constitutively active RB allele refractory to phosphorylation (PSM.7-LP) (Knudsen and Wang, 1997) indicated RB activity was sufficient to induce the accumulation of mitochondria in a manner comparable to PD-0332991 (Figure 1G). It has recently been shown that RB can associate with mitochondria (Hilgendorf et al., 2013). However, in the presence of the CDK4/6 inhibitor, RB was solely nuclear as determined by immunofluorescence microscopy (Figure S1). In parallel with these established cell lines, PD-0332991 treatment of a low passage patient-derived PDA cell line elicited a similar increase in MitoTracker (Figure 1H). To determine whether these effects were observed in vivo, the matched xenograft model derived from the same patient was treated with PD-0332991 for 8 days. This treatment elicited potent suppression of Ki67, consistent with the established role for CDK4/6; and as observed in cell lines, there was an increase in mitochondria (Figure 1I).

Reprogramming of Metabolism with CDK4/6 Inhibition

To determine the effect of increased mitochondria number on metabolism, oxygen consumption was evaluated as a measure of increased oxidative phosphorylation. As shown in Figure 2A, there was a substantial increase in oxidative phosphorylation with CDK4/6 inhibition. Analysis of metabolite levels in culture media indicated that PD-0332991 treatment resulted in a significant increase in glucose and glutamine consumption. Correspondingly, there was enhanced glutamate secretion as a product of glutamine metabolism, and increased lactate efflux as a measure of the end product of glycolysis (Figure 2B). Consistent with the increase in lactate production, there was a significant increase in media acidification (Figure 2C). These features were recapitulated with LEE-011 and LY2853219, indicating that increased metabolism is a general feature of CDK4/6

Figure 1. CDK4/6 Inhibition Leads to Mitochondria Accumulation in an RB-Dependent Fashion

(A) Representative flow cytometry histogram displaying cellular complexity on the x axis for cells treated with PD-0332991 for 120 hr.

(B) Relative ATP levels from cells treated with control or PD-0332991 for 120 hr. The average and SD are shown, and the statistical comparison to vehicle control was determined by t test (**$p < 0.01$, ***$p < 0.001$).

(C) Confocal fluorescence imaging of mitochondria (62.5×) in the indicated cells treated with PD-0332991 for 120 hr (scale bar, 20 μm).

(D) Flow cytometry histograms showing comparison of MitoTracker red fluorescence of the control versus PD-0332991-treated cells.

(E) Representative transmission electron microscope micrograph of control and PD-0332991-treated PL5 cells (scale bar, 1 μm). Quantification of mitochondria from counting high-power fields and the average and SD are shown. The statistical comparison to vehicle control was determined by t test (***$p < 0.001$).

(F) Flow cytometry histograms showing comparison of MitoTracker red fluorescence of the control versus PD-0332991-treated cells following CCND1 or RB knockdown.

(G) Quantitation of MitoTracker red intensity following treatment with PD-0332991 or transduction of the constitutively active RB allele 7-LP. The average and SD are shown. The statistical comparison to vehicle control was determined by t test (*$p < 0.05$, **$p < 0.01$).

(H) Flow cytometry histograms showing comparison of MitoTracker red fluorescence of the control versus PD-0332991-treated cells in the EMC43 cell model.

(I) H&E staining, immunohistochemistry for (Ki67) (scale bar, 100 μm), and fluorescence (scale bar, 200 μm) imaging (TOM20/Vimentin/DAPI) of patient-derived xenograft EMC43.

See also Figure S1.

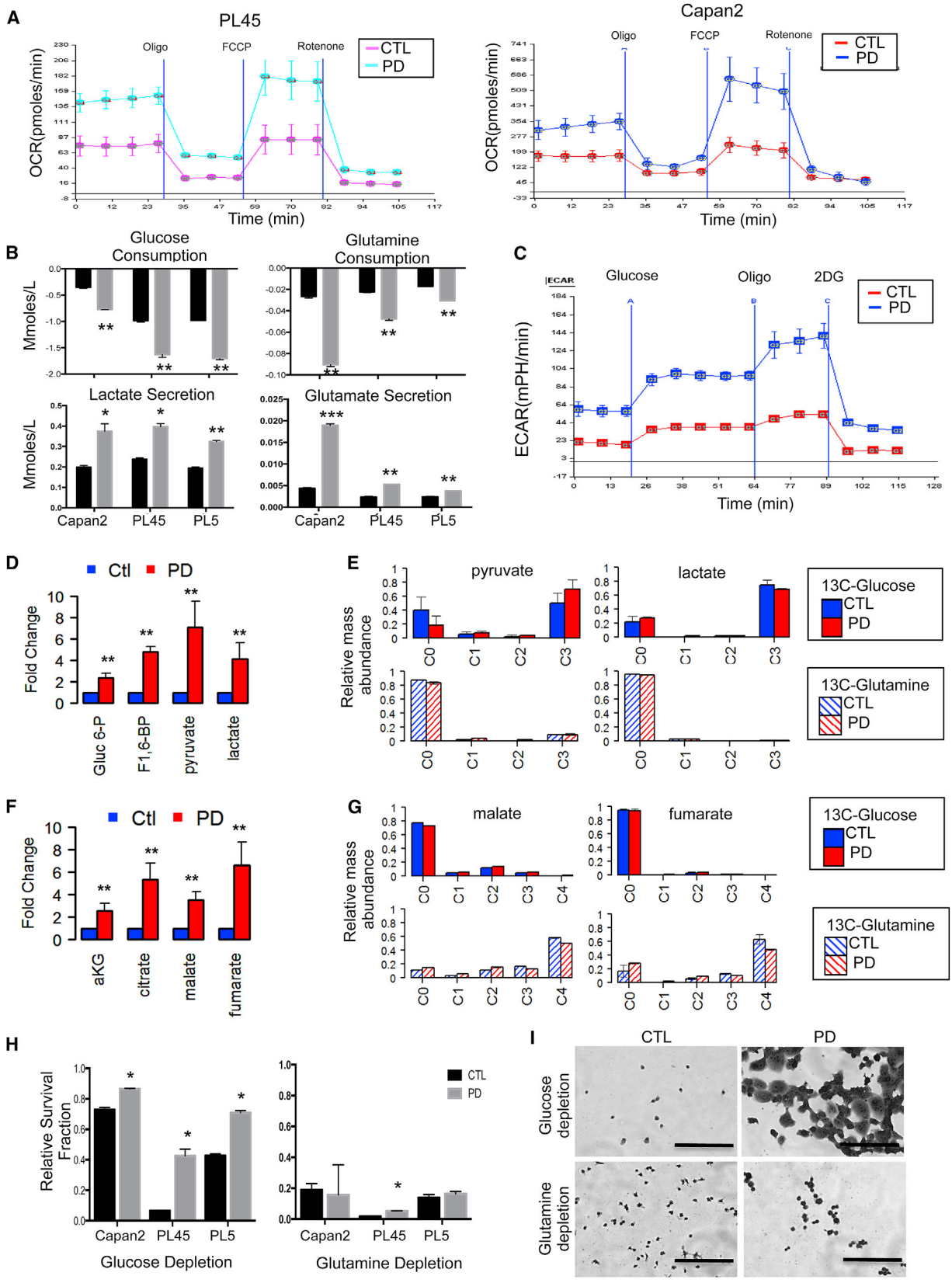

(legend on next page)

inhibition (Figure S2). Metabolomic analysis was performed in conjunction with universally labeled 13C-glucose and 13C-glutamine to monitor metabolic flux. These analyses showed increase in glycolytic intermediates (i.e., glucose 6-phosphate, fructose 1,6-bisphosphate, pyruvate, and lactate) that were predominantly derived from glucose as expected (Figure 2E). For TCA metabolites (i.e., malate, fumarate, succinate, and alpha-ketoglutarate), there were also significant increases in metabolite levels (Figure 2F). Flux analysis indicated that these metabolites were principally derived from glutamine; therefore, the majority of mitochondrial-derived metabolism is fueled by glutamine in these models (Figure 2G). Starving cells of either glutamine or glucose significantly reduced viability (Figures 2H and 2I). However, pretreatment with CDK4/6 inhibitors protected selectively against the effect of acute glucose withdrawal, suggesting that enhanced glutamine metabolism was sufficient to rescue the reliance on glucose. Similarly, CDK4/6 inhibition limited the acute toxicity of mitochondrial inhibitors phenformin and rotenone (Figure S2). These findings underscore the possibility that the metabolic status of CDK4/6-treated cells could impact on tumor biology and therapeutic sensitivities.

CDK4/6 Inhibition Drives MTOR Pathway Activation

Given the significance of signaling pathways in regulating metabolism, we assessed how CDK4/6 inhibition influences the levels of 217 protein and phospho-proteins by reverse phase protein array (RPPA) analysis (Tibes et al., 2006) (Figure 3A). Interestingly, there were very few significant changes in protein abundance mediated by CDK4/6 inhibition. In terms of downregulated proteins, phosphorylated RB and E2F targets (e.g., Cyclin B1) were downregulated as expected (Figure 3A). In contrast, the phosphorylation of ribosomal protein S6 at Ser235/236 was uniquely observed to be significantly increased with CDK4/6 inhibition (Figure 3A). Immunoblotting confirmed the increased phosphorylation of S6, an MTOR complex 1 (TORC1) substrate, and also increased phosphorylation of RSK at Ser 389 (Figure 3B). In contrast, there was no increase in either ERK or AKT phosphorylation (Figure 3B). To determine if this signaling feature of CDK4/6 inhibition is observed in vivo, tumor sections from xenografts treated with PD-0332991 were stained for Ki67 and phosphorylated S6 and showed the expected reduction in Ki67 and a significant increase in S6 phosphorylation (Figure 3C). Similar results were observed in PDX models (Figure S3). Together, these data indicate that MTOR signaling is activated with the inhibition of CDK4/6. Parallel analysis of transcriptional pathways was performed on cells treated with PD-0332991 for 5 days. This treatment resulted in the downregulation of multiple genes involved in cell-cycle control, consistent with the expected suppression of RB phosphorylation (Figures 3D and S3). However, a large number of genes were significantly upregulated (Figure 3D), and gene set enrichment analysis identified the induction of genes associated with glycolysis, lysosome, pyruvate metabolism, fatty acid metabolism, and PPAR signaling (Figures 3D and S3). Importantly, many of these processes are activated downstream of MTOR (Laplante and Sabatini, 2009), suggesting this signaling pathway is associated with CDK4/6-inhibition-mediated metabolic effects.

Canonically, the activation state of MTOR is regulated by PI3K/AKT/TSC pathway, amino acid availability, lysosomes, and the appropriate milieu of regulatory proteins (Laplante and Sabatini, 2012). In the analysis of gene expression data and RPPA, there was no evidence for the activation of PI3K/AKT or the abundance of TORC1 or TORC2 subunits or regulatory proteins (not shown). However, there was a rapid (24 hr) increase in lysosomes that preceded the increase in mitochondria (Figure S3). Immunofluorescence analysis demonstrated that the majority of MTOR in PDA models is associated with lysosomal structures, and treatment with CDK4/6 inhibitors increased lysosome-associated MTOR (Figure S3). These data suggest that TORC1 complex activation is occurring. Additionally, there was an accumulation of amino acids as determined by mass spectrometry (Figure S3). Consistent with the supposition that amino acids play an important role downstream from RB, depletion of amino acids blocked the induction of MTOR activity with CDK4/6 inhibition (Figure S3). Together, these data suggest that CDK4/6 inhibition triggers an energetic feedforward loop that engages MTOR signaling for metabolic reprogramming.

MTOR and MEK Inhibitors Exhibit Distinct Endpoints with CDK4/6 Inhibition

To determine the functional interaction between CDK4/6 inhibition and signaling pathways, a panel of agents that inhibit

Figure 2. CDK4/6 Inhibition Leads to Metabolic Reprogramming

(A) Oxygen consumption rate (OCR) of PL45 and Capan2 cell lines either control or treated with PD-0332991.

(B) Quantification of media glucose and glutamine uptake, and glutamate and lactate production from the indicated cell lines with or without PD-0332991 treatment. The average and SD are shown. The statistical comparison to vehicle control was determined by t test (*$p < 0.05$, **$p < 0.01$, ***$p < 0.001$).

(C) Extracellular acidification rate (ECAR) in cells treated with or without PD-0332991.

(D) Relative fold change of glycolytic intermediates Glucose 6P; Fructose 1,6BP; pyruvate; and lactate as determined by mass spectrometry. The average and SD are shown. The statistical comparison to vehicle control was determined by t test.

(E) Flux analysis of cell populations treated with universally labeled 13C-glucose (solid bars) or universally labeled 13C-glutamine (stippled bars). Bars show the relative average abundance and SD of differing mass species.

(F) Relative fold change of TCA intermediates alpha-ketoglutare, citrate, malate, and fumarate. The average and SD are shown. The statistical comparison to vehicle control was determined by t test (**$p < 0.01$).

(G) Flux analysis of cell populations treated with universally labeled 13C-glucose (solid bars) or universally labeled 13C-glutamine (stippled bars). Bars show the relative average abundance and SD of differing mass species.

(H) Quantification of cell viability following acute glucose or glutamine withdrawal. The average and SD are shown. The statistical comparison to vehicle control was determined by t test (*$p < 0.05$).

(I) Representative images of crystal violet stained cells following either glutamine or glucose withdrawal (scale bar, 200 μm).

See also Figure S2.

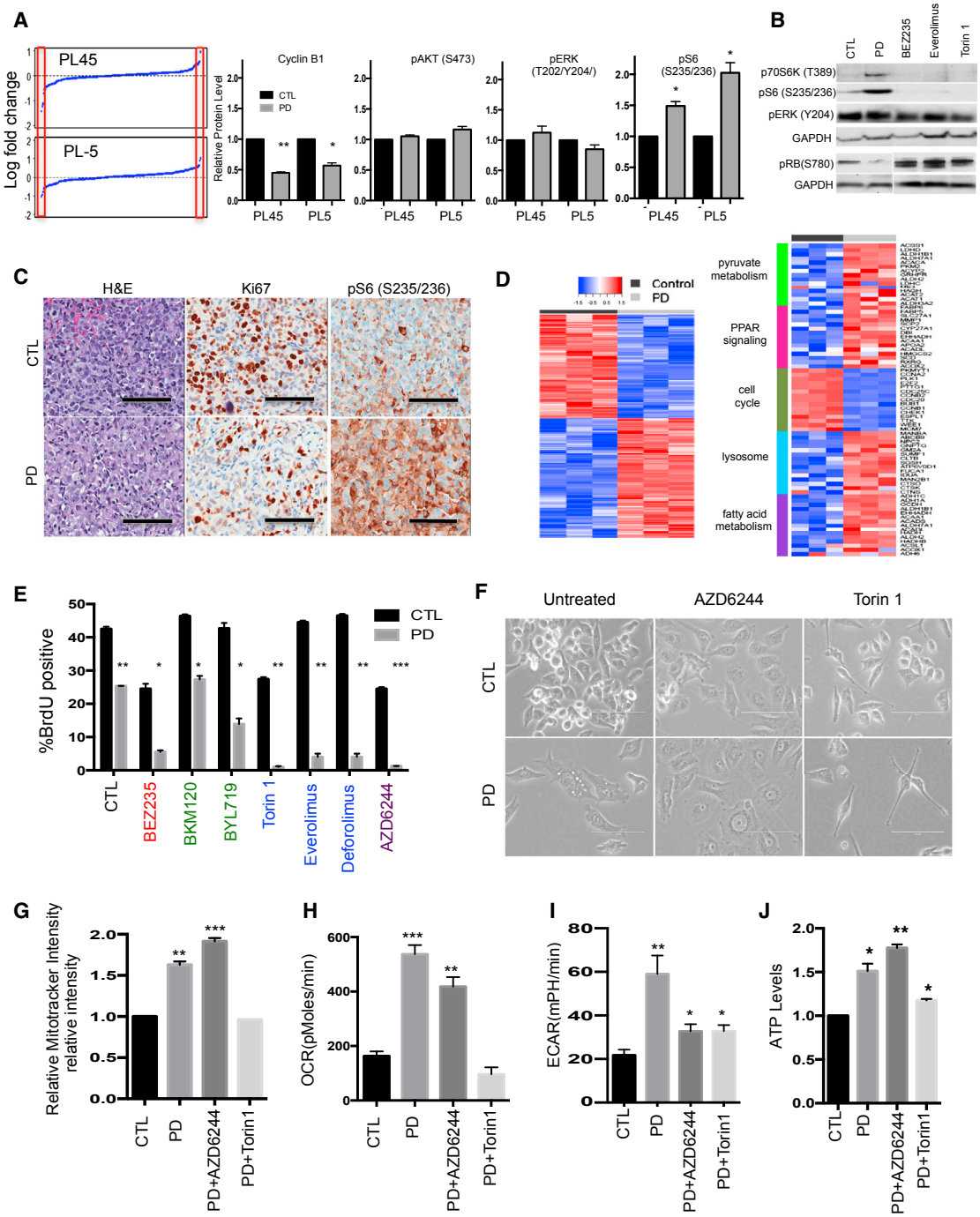

Figure 3. CDK4/6 Inhibition Leads to the Induction of MTOR Activity and Downstream Effects on Metabolism

(A) Quantification of reverse phase protein array (RPPA) data. The log-fold change of proteins abundance with PD-0332991 treatment is displayed as a function of the 217 protein species detected on the array. RPPA data for selected proteins and phosphoproteins is shown, with the average abundance and SD. The statistical comparison to vehicle control was determined by t test (*$p < 0.05$, **$p < 0.01$).

(B) Immunoblotting was performed for the indicated proteins in cells treated with the indicated pathway selective inhibitors.

(C) Immunohistochemical analysis of xenograft tumors treated with lactate control or PD-0332991 for 8 days. Representative images of Ki67 and pS6 (S235/236) are shown (scale bar, 100 μm).

(D) Gene expression profiling was performed on Capan 2 cells treated with control or PD-0332991 for 120 hr. The heatmap shows genes passing a 1.5-fold $p < 0.05$ cutoff. Representative genes falling into selected gene set enrichment categories are shown in the heatmap.

(legend continued on next page)

PI3K, MTOR, and MEK was employed. Consistent with prior work (Franco et al., 2014), we observed potent cooperation of MTOR and MEK inhibitors with CDK4/6 inhibitors; however, there was little influence of PI3K selective inhibitors (Figure 3E). Interestingly, there were significant differences in the morphology of cells treated with MEK versus MTOR inhibitors (Figure 3F). Since both MTOR and MEK inhibitors cooperated to invoke similar levels of cell-cycle inhibition, the associated influence on metabolism was evaluated. MEK inhibition further augmented the impact of CDK4/6 inhibition on oxidative metabolism including increased mitochondrial mass, cellular complexity, and enhanced OCR (Figures 3G, 3H, and S3). However, MEK inhibition selectively inhibited glycolysis (Figure 3I). In contrast, combined CDK4/6 and MTOR inhibition resulted in the suppression of both glycolytic and oxidative functions, as was most evident in terms of the mitochondrial accumulation that was completely suppressed (Figures 3G–3I and S3). These combined findings suggest a pathway through which the selective activation of RB in the presence of oncogenic signals enables the further accumulation of MTOR signaling and resultant stimulation of metabolism, while MEK is predominantly required for the maintenance of glycolytic metabolism.

Combination Treatments with CDK4/6 Inhibitors Result in Durable Therapeutic Response

The distal effects of the combination of CDK4/6 inhibition with MTOR or MEK inhibition were evaluated. MEK in combination with CDK4/6 inhibition enforced profound cell-cycle inhibition (Figure S4) and a potent cytostatic effect with evidence of induced senescence (SA-β-Gal) (Figure 4A). In contrast, MTOR inhibition suppressed senescence, but resulted in the induction of cell death (Figure 4B). This apoptotic cell death could not be reversed by supplementation with methyl-pyruvate or alpha-ketoglutarate, which directly supports mitochondrial metabolism (Figure S4). The treatment yielded suppression of tumor cell proliferation over > 2 weeks in culture (Figure 4C). Importantly, in PL5 xenograft models while both PD-0332991 and the PI3K/MTOR inhibitor BEZ235 exhibit some single agent activity, the combination was significantly more potent for the suppression of tumor cell growth and proliferative index (Figures 4D, 4E, and S4). These data were further confirmed through the use of an independent orthotopic model (PL45), where the combined treatment both suppressed tumor growth and reduced metastatic burden in this highly aggressive model (Figures 4E and S4).

Selectively Targeting ROS and Mitochondria in the Presence of CDK4/6 Inhibition

A high level of oxidative phosphorylation is believed to represent a liability to tumor cells, due to the role of mitochondria in apoptosis and generation of reactive oxygen species (ROS). Indeed, treatment of the PDA models with CDK4/6 inhibitor resulted in increased total ROS and mitochondria-derived ROS (Figure 4F and S4). However, one of the key transcriptional responses to CDK4/6 inhibition includes the accumulation of genes involved in peroxisome biosynthesis and the expression of ROS scavengers including hemeoxygenase 1 (HO-1) and catalase (CAT) (Figure S4). The knockdown of either HO-1 or CAT elicited a significant reduction in PDA cell growth and cooperated with CDK4/6 inhibition (Figures 4G, 4H, and S4). These findings suggest that increased utilization of mitochondria is balanced by antioxidant pathways in the context of CDK4/6 inhibition. Interestingly, not all perturbations of ROS regulatory processes cooperated with CDK4/6 inhibition. Notably, the glutathione inhibitor BSO failed to further increase ROS levels above CDK4/6 inhibition and similarly did not cooperate with CDK4/6 inhibition in these models (Figure S4).

An alternative means to exploit mitochondria is through mobilization of BH3-containing proteins. It is known that ROS and other stresses, including CDK inhibition, can effectively limit the expression of MCL1 or modify its activity (Brunelle et al., 2007; Thomas et al., 2010). Cells treated with PD-0332991 exhibited a marked suppression of the high-mobility form of MCL1 (Figure S4). To determine whether this was related to increased sensitivity to mitochondrial-mediated apoptosis, the BCL2 inhibitor ABT-737 was employed (Oltersdorf et al., 2005). Cells that had been pretreated with PD-0332991 and exhibited an accumulation of mitochondria were selectively sensitive to ABT-737 that elicited apoptotic cell death (Figures 4J–4L and S4). Importantly, the pretreatment with CDK4/6 inhibition also elicited long-term suppression of proliferation in combination with ABT-737 (Figure 4L). Together, these data indicate that the mitochondria and metabolic features of CDK4/6 treated cells could be selectively exploited to yield a synthetic approach to cancer treatment.

DISCUSSION

There has been an ever-increasing appreciation of the importance of metabolism in cancer and as a target for therapeutic intervention (Sousa and Kimmelman, 2014; Vander Heiden, 2011). In parallel, it is becoming evident that CDK4/6 inhibitors will be utilized in multiple clinical settings either singly or in combination (Asghar et al., 2015; Dickson, 2014).

The impact of CDK4/6 inhibition on tumor metabolism is distinct from other targeted agents that have been evaluated in PDA models. In general, therapeutic agents against the KRAS signaling pathway suppress features of mitogenic signaling and result in attenuation of specific facets of

(E) Quantification of BrdU positive cells following 24 hr treatment with dual PI3K/MTOR (BEZ235), PI3K (BKM120, BYL719), mTOR (Torin, Everolimus, and Deforolimus), and MEK (AZD-6244) inhibitors alone and in combination with PD-0332991 treatment. The average BrdU incorporation and SD are shown. The statistical comparison to single agent treatment was determined by t test (*$p < 0.05$, **$p < 0.01$, ***$p < 0.001$).
(F) Bright-field images of PD-0332991, AZD-6244, and Torin 1 and combination treated cells (scale bar, 100 μm).
(G–J) Quantification of mitochondria (G), OCR (H), ECAR (I), and ATP (J) levels from cells treated with the indicated drugs and combinations. The average signals and SD are shown. The statistical comparison to control was determined by t test (*$p < 0.05$, **$p < 0.01$, ***$p < 0.001$).
See also Figure S3.

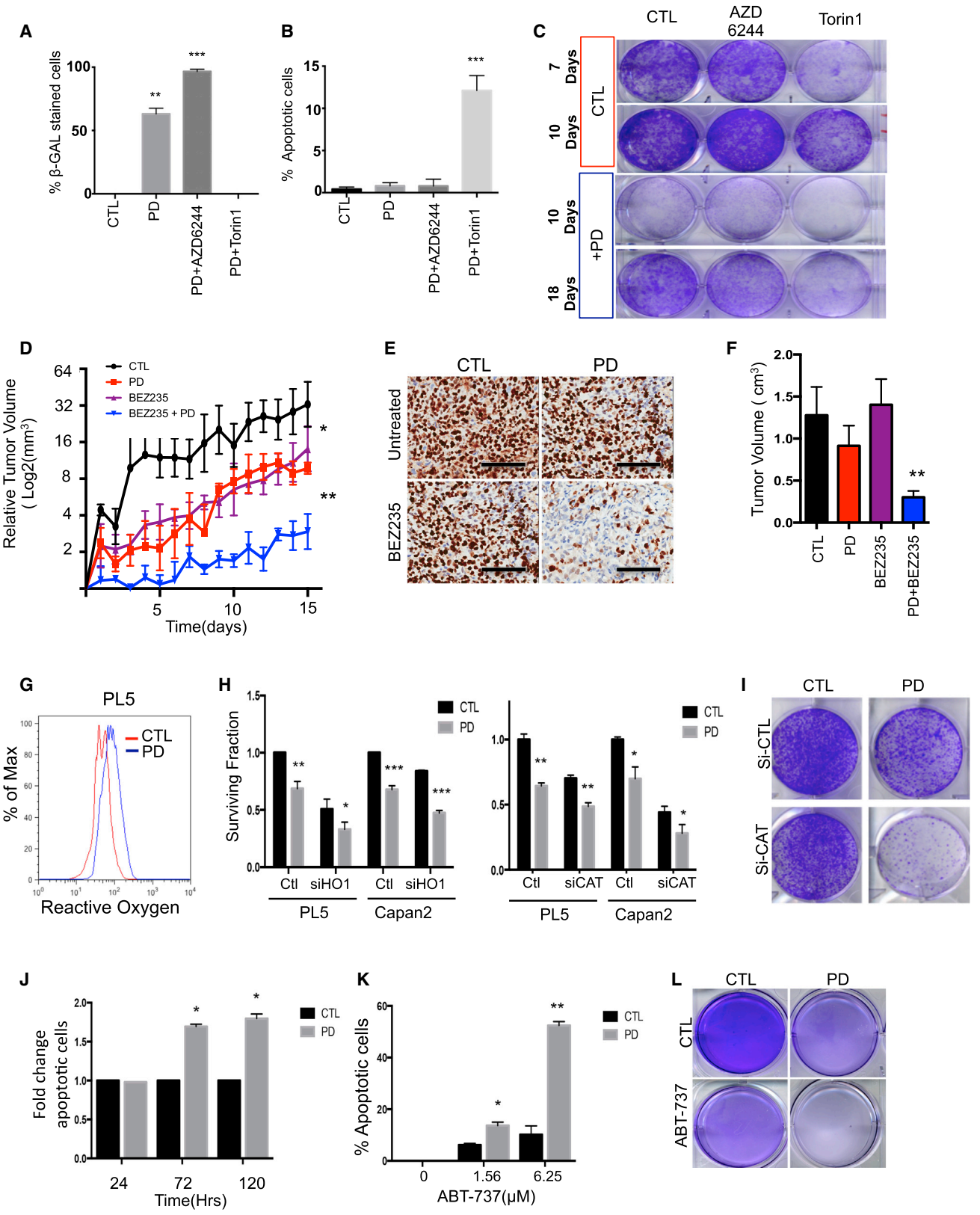

(legend on next page)

metabolic activity (Lyssiotis et al., 2013; Vander Heiden, 2011; Viale et al., 2014; Ying et al., 2012). This can occur either through the attenuation of glycolysis as observed with MEK inhibitors, or a general diminution of metabolic function as reported with MTOR inhibitors. Increased metabolic activity observed in PDA models with CDK4/6 inhibition was surprising, since in different settings CDK4 and Cyclin D1 expression or RB loss enhance metabolic functions associated with proliferation (Clem and Chesney, 2012; Lopez-Mejia and Fajas, 2015; Reynolds et al., 2014). For example, in *Drosophila* CDK4 is well-established to drive cellular growth by activating metabolic pathways (Datar et al., 2000). In spite of these prior studies, recent work has shown that RB loss is selectively associated with a diminution of oxidative phosphorylation and increased sensitivity to mitochondrial poisons (Nicolay et al., 2015). Therefore, our findings suggest that RB activation by CDK4/6 inhibition essentially drives this process in reverse and activates mitochondrial function. Correspondingly, such treated cells are actually less sensitive to glucose withdrawal and mitochondrial poisons.

The finding that tumors treated with CDK4/6 inhibitors maintain a high metabolic rate has significant clinical implications. Such a state could represent a potential liability as the treated tumor cells are metabolically charged for cell division, and cessation of the CDK4/6 inhibition could elicit rapid cell-cycle progression. In yeast models the accumulation of cell mass and energetics can drive subsequent rounds of proliferation under non-ideal conditions (Cai and Tu, 2012). This could in part represent one of the challenges of employing CDK4/6 inhibitors as single agents in the clinic. Importantly, the metabolic features observed here in preclinical models are consistent with imaging from clinical trials. In the analysis of single agent PD-0332991 in mantle cell lymphoma, the FLT-PET signal, which measures thymidine utilization, was suppressed, while the signal for FDG-PET was maintained, suggesting the tumors treated in this fashion maintain significant metabolic activity (Leonard et al., 2012).

Mechanistically, CDK4/6 inhibitors are unique as they suppress proliferation downstream from many of the oncogenic signaling pathways that stimulate both metabolism and cellular proliferation (Asghar et al., 2015; Dickson, 2014). As shown here, the activity of effectors distal to KRAS is maintained following the exposure to CDK4/6 inhibitor. Additionally, we find MTOR signaling is stimulated with suppression of CDK4/6 activity in the PDA cells and tumor models studied. MTOR engages a signaling program downstream from nutrient availability to stimulate metabolism leading to cell-cycle progression (Laplante and Sabatini, 2009, 2012) and therefore is generally antagonistic to the cytostatic effect of CDK4/6 inhibition. We observe the induction of multiple gene expression programs known to be downstream of MTOR including glycolysis, lysosome biogenesis, fatty acid metabolism, and PPAR signaling (Laplante and Sabatini, 2009). Presumably this elevated MTOR signaling in concert with a suppression of cell-cycle progression is sufficient to enhance the metabolic features observed in the PDA cultures and tumors observed. One of the key questions is how CDK4/6 impacts MTOR. MTOR activation occurs as a consequence of amino acid availability and lysosomal localization (Sancak et al., 2008). Interestingly, CDK4/6 inhibition yielded a rapid accumulation of lysosomes, and metabolomics analysis showed increased amino acid pools. These data suggest an energetic feedforward loop, wherein CDK4/6 inhibition yields increased metabolic activity that is further exaggerated by MTOR activation that mediates downstream effects on metabolism and mitochondria. Critically, MTOR inhibition can suppress effects of CDK4/6 inhibitor on metabolism; thus, MTOR activity is required for metabolic reprogramming induced by CDK4/6 inhibition. In spite of these findings, the exact signaling through which CDK4/6 and RB controls metabolism remains under study, as does the potential context dependence beyond the PDA models studied here.

In pancreatic and other solid tumors, the efficacy of CDK4/6 inhibitors will likely be dependent on combination therapies. Thus, defining means to selectively capitalize on the metabolic status

Figure 4. Selective Cooperation with CDK4/6 Inhibition for Enhancing Therapeutic Effect

(A) Quantification of SA-β-gal positive cells following the indicated treatments. The average number of senescent cells and SD are shown. The statistical comparison to control was determined by t test (**$p < 0.01$, ***$p < 0.001$).

(B) Quantification of apoptotic cells following the indicated treatments. The average number of apoptotic cells and SD are shown. The statistical comparison to control was determined by t test (***$p < 0.001$).

(C) Colony formation was assessed at the indicated times by crystal violet staining. Representative images are shown.

(D) Tumor volume of PL5 xenografts following treatment with BEZ235, PD-0332991, and the combination was measured as a function of time. The average volume and SD are plotted, and the statistical comparison versus vehicle treated control is shown by t test (*$p < 0.05$, **$p < 0.01$).

(E) Representative Ki-67 immunohistochemistry of the PL5 treated xenografts (scale bar, 100 μm).

(F) Tumor volume of orthotopically implanted PL45 cells that were treated with the indicated agents. The average volume, SD, and statistical comparison to the vehicle treated control are shown.

(G) Representative histograms showing fluorescence of total ROS in the presence versus absence of PD-0332991.

(H) Surviving cells following HO-1 or CAT knockdown in the absence or presence of PD-0332991 was determined. Bars show the average surviving fraction relative to transfected controls. The statistical analysis to the RNAi control was determined by t test (*$p < 0.05$, **$p < 0.01$, ***$p < 0.001$).

(I) Colony outgrowth of knockdown cells alone or in combination with PD-0332991. Representative images are shown.

(J) Fold change in fraction of apoptotic cells pretreated with PD-0332991 for the indicated period of time, followed by acute treatment with ABT-737. The average number of apoptotic cells and standard SD are shown. The statistical analysis to single agent versus combination with PD-0332991 was determined by t test (*$p < 0.05$).

(K) Impact of PD-0332991 pretreatment on sensitivity to ABT-737. The average and SD are shown. The statistical comparison to control was determined by t test (*$p < 0.05$, **$p < 0.01$).

(L) Prolonged treatment with ABT-737 of control or PD-0332991 pretreated and stained for crystal violet.

See also Figure S4.

imparted by CDK4/6 inhibition is particularly pertinent. Due to the withdrawal from the cell cycle, CDK4/6 inhibitors have an antagonistic function related to select chemotherapies (Roberts et al., 2012), further underscoring the need for rational combinatorial approaches. In breast cancer models, PI3K inhibitors potently cooperate with CDK4/6 inhibition (Vora et al., 2014). However, this combination has a relatively modest effect in PDA models. In contrast, MEK and MTOR inhibition potently cooperate with CDK4/6 inhibition (Franco et al., 2014; Heilmann et al., 2014). In spite of similar effects on cell-cycle suppression, MEK and MTOR inhibition have distinct effects on metabolism and biology. As has been previously published, MEK activity is particularly relevant for maintaining glycolytic function in PDA models (Ying et al., 2012). MEK inhibitors function in concert with CDK4/6 inhibition to enhance the accumulation of mitochondria and oxidative phosphorylation, eliciting a pronounced cell-cycle arrest with features of senescence. In contrast, MTOR inhibitors restricted glycolytic metabolism and oxidative phosphorylation induced by CDK4/6 inhibition and yielded cell death and suppression of tumor growth. While potent cooperation is observed in several cell and xenograft models, a concerted effort across multiple patient-derived models will be required to determine the fraction of tumors that would be expected to be sensitive to such interventions in the clinic.

Targeting metabolism or other conserved features of cell biology represents a challenge in establishing a therapeutic index (Galluzzi et al., 2013). In contrast with other agents, the increase in tumor associated mitochondria and ROS could represent a unique target for tumors treated with CDK4/6 inhibitors (Sabharwal and Schumacker, 2014). Inhibitors of antioxidants are being considered as cancer therapies due to the established increase in ROS production by many tumors (Gorrini et al., 2013). We observed that both depletion of catalase or hemoxygenase-1 cooperated with CDK4/6 inhibition. Similarly, the high levels of mitochondria in principle could yield increased sensitivity to mitochondrial-driven cell death mediated by agents such as ABT-737. Thus, these studies provide potential avenues for considering converting the cytostatic nature of CDK4/6 inhibitors to cytotoxicity.

Given the recent FDA approval of CDK4/6 inhibitors, their use will become progressively commonplace. Understanding both canonical cell-cycle and metabolic features of treatment exposure will be important for defining preferred combination strategies and capitalizing on tumor biology.

EXPERIMENTAL PROCEDURES

Cell Culture and Transfections

The established cell lines Capan2, PL45, and PL5 were cultured as previously described (Franco et al., 2014). Primary cell lines (EMC43, EMC18128, and EMC7310) were cultured in keratinocyte serum-free (KSF) medium with 0.2 ng/ml EGF and 30 μg/ml bovine pituitary extract (Invitrogen) on collagen-coated plates. Cells were transfected with RNAi or transduced with adenoviruses as previously described (Baek et al., 2014; Franco et al., 2014). Detailed descriptions are provided in the Supplemental Experimental Procedures.

Mitochondria and Lysosome Analysis

Staining of mitochondria with MitoTracker and LysoTracker was as previously described (Baek et al., 2014). The transmission electron microscopy and staining is described in detail in the Supplemental Experimental Procedures.

Immunoblotting, Immunohistochemistry, and Immunofluorescence

For immunoblotting total cell extracts were prepared, resolved by SDS-PAGE, and transferred to immobilon membranes. The following primary antibodies were utilized from the indicated vendors: pRB (S780), total RB, p-p70s6k (T389), pAKT (S473), pERK (Y204), pS6 (S235/236), and MTOR were from Cell Signaling Technology; VDAC and Vimentin were from Abcam; GAPDH, LAMP-2, Cyclin A, Catalase, and Tom20 antibodies were from Santa Cruz; Cyclin D1 was from Neomarkers; and HMOX1 was from Millipore. Immunohistochemistry and immunofluorescence staining were performed as described in detail in the Supplemental Experimental Procedures.

Metabolic Analysis

Glucose and glutamine uptake and lactate and glutamate production was assessed using a biochemistry analyzer (BioProfile Basic 4 Analyzer; Nova Biomedical). Measurement of oxygen consumption rate and extracellular acidification rates were performed using a Seahorse Bioscience XF24 Extracellular Flux Analyzer. Metabolite levels were determined using a Q Exactive benchtop Orbitrap mass spectrometer equipped with an Ion Max source and a HESI II probe, which was coupled to a Dionex UltiMate 3000 UPLC system (Thermo Fisher Scientific). A detailed description of these approaches is provided in the Supplemental Experimental Procedures.

SUPPLEMENTAL INFORMATION

Supplemental Information includes Supplemental Experimental Procedures and four figures and can be found with this article online at http://dx.doi.org/10.1016/j.celrep.2015.12.094.

AUTHOR CONTRIBUTIONS

Conceptualization, A.K.W. and E.S.K.; Methodology, U.B., A.K.W., E.S.K., E.F., and J.F.; Formal Analysis, U.B. and J.F.; Investigation, J.F., A.K.W., E.F., and U.B.; Writing, E.S.K., A.K.W., and J.F.; Supervision and Funding, E.S.K. and A.K.W.

ACKNOWLEDGMENTS

The authors thank their colleagues for thought-provoking discussion and assistance with manuscript development. Cody Eslinger provided specific technical assistance on the primary cell models, the UT Shared Tissue Resource provided support for histological and tissue staining, and Dr. Ralph DeBerardinis provided access to equipment and expertise. This study was supported by grants from NIH.

Received: August 25, 2015
Revised: November 23, 2015
Accepted: December 19, 2015
Published: January 21, 2016

REFERENCES

Ambrus, A.M., Islam, A.B., Holmes, K.B., Moon, N.S., Lopez-Bigas, N., Benevolenskaya, E.V., and Frolov, M.V. (2013). Loss of dE2F compromises mitochondrial function. Dev. Cell *27*, 438–451.

Asghar, U., Witkiewicz, A.K., Turner, N.C., and Knudsen, E.S. (2015). The history and future of targeting cyclin-dependent kinases in cancer therapy. Nat. Rev. Drug Discov. *14*, 130–146.

Baek, G., Tse, Y.F., Hu, Z., Cox, D., Buboltz, N., McCue, P., Yeo, C.J., White, M.A., DeBerardinis, R.J., Knudsen, E.S., and Witkiewicz, A.K. (2014). MCT4 defines a glycolytic subtype of pancreatic cancer with poor prognosis and unique metabolic dependencies. Cell Rep. *9*, 2233–2249.

Benevolenskaya, E.V., and Frolov, M.V. (2015). Emerging links between E2F control and mitochondrial function. Cancer Res. *75*, 619–623.

Blanchet, E., Annicotte, J.S., Lagarrigue, S., Aguilar, V., Clapé, C., Chavey, C., Fritz, V., Casas, F., Apparailly, F., Auwerx, J., and Fajas, L. (2011). E2F transcription factor-1 regulates oxidative metabolism. Nat. Cell Biol. *13*, 1146–1152.

Brunelle, J.K., Shroff, E.H., Perlman, H., Strasser, A., Moraes, C.T., Flavell, R.A., Danial, N.N., Keith, B., Thompson, C.B., and Chandel, N.S. (2007). Loss of Mcl-1 protein and inhibition of electron transport chain together induce anoxic cell death. Mol. Cell. Biol. *27*, 1222–1235.

Bryant, K.L., Mancias, J.D., Kimmelman, A.C., and Der, C.J. (2014). KRAS: feeding pancreatic cancer proliferation. Trends Biochem. Sci. *39*, 91–100.

Cai, L., and Tu, B.P. (2012). Driving the cell cycle through metabolism. Annu. Rev. Cell Dev. Biol. *28*, 59–87.

Chicas, A., Wang, X., Zhang, C., McCurrach, M., Zhao, Z., Mert, O., Dickins, R.A., Narita, M., Zhang, M., and Lowe, S.W. (2010). Dissecting the unique role of the retinoblastoma tumor suppressor during cellular senescence. Cancer Cell *17*, 376–387.

Clem, B.F., and Chesney, J. (2012). Molecular pathways: regulation of metabolism by RB. Clin. Cancer Res. *18*, 6096–6100.

Datar, S.A., Jacobs, H.W., de la Cruz, A.F., Lehner, C.F., and Edgar, B.A. (2000). The Drosophila cyclin D-Cdk4 complex promotes cellular growth. EMBO J. *19*, 4543–4554.

Dean, J.L., Thangavel, C., McClendon, A.K., Reed, C.A., and Knudsen, E.S. (2010). Therapeutic CDK4/6 inhibition in breast cancer: key mechanisms of response and failure. Oncogene *29*, 4018–4032.

Dickson, M.A. (2014). Molecular pathways: CDK4 inhibitors for cancer therapy. Clin. Cancer Res. *20*, 3379–3383.

Franco, J., Witkiewicz, A.K., and Knudsen, E.S. (2014). CDK4/6 inhibitors have potent activity in combination with pathway selective therapeutic agents in models of pancreatic cancer. Oncotarget *5*, 6512–6525.

Fry, D.W., Harvey, P.J., Keller, P.R., Elliott, W.L., Meade, M., Trachet, E., Albassam, M., Zheng, X., Leopold, W.R., Pryer, N.K., and Toogood, P.L. (2004). Specific inhibition of cyclin-dependent kinase 4/6 by PD 0332991 and associated antitumor activity in human tumor xenografts. Mol. Cancer Ther. *3*, 1427–1438.

Galluzzi, L., Kepp, O., Vander Heiden, M.G., and Kroemer, G. (2013). Metabolic targets for cancer therapy. Nat. Rev. Drug Discov. *12*, 829–846.

Gorrini, C., Harris, I.S., and Mak, T.W. (2013). Modulation of oxidative stress as an anticancer strategy. Nat. Rev. Drug Discov. *12*, 931–947.

Heilmann, A.M., Perera, R.M., Ecker, V., Nicolay, B.N., Bardeesy, N., Benes, C.H., and Dyson, N.J. (2014). CDK4/6 and IGF1 receptor inhibitors synergize to suppress the growth of p16INK4A-deficient pancreatic cancers. Cancer Res. *74*, 3947–3958.

Hilgendorf, K.I., Leshchiner, E.S., Nedelcu, S., Maynard, M.A., Calo, E., Ianari, A., Walensky, L.D., and Lees, J.A. (2013). The retinoblastoma protein induces apoptosis directly at the mitochondria. Genes Dev. *27*, 1003–1015.

Knudsen, E.S., and Wang, J.Y. (1997). Dual mechanisms for the inhibition of E2F binding to RB by cyclin-dependent kinase-mediated RB phosphorylation. Mol. Cell. Biol. *17*, 5771–5783.

Lamb, J., Ramaswamy, S., Ford, H.L., Contreras, B., Martinez, R.V., Kittrell, F.S., Zahnow, C.A., Patterson, N., Golub, T.R., and Ewen, M.E. (2003). A mechanism of cyclin D1 action encoded in the patterns of gene expression in human cancer. Cell *114*, 323–334.

LaPak, K.M., and Burd, C.E. (2014). The molecular balancing act of p16(INK4a) in cancer and aging. Mol. Cancer Res. *12*, 167–183.

Laplante, M., and Sabatini, D.M. (2009). mTOR signaling at a glance. J. Cell Sci. *122*, 3589–3594.

Laplante, M., and Sabatini, D.M. (2012). mTOR Signaling. Cold Spring Harb. Perspect. Biol. *4*, a011593.

Leonard, J.P., LaCasce, A.S., Smith, M.R., Noy, A., Chirieac, L.R., Rodig, S.J., Yu, J.Q., Vallabhajosula, S., Schoder, H., English, P., et al. (2012). Selective CDK4/6 inhibition with tumor responses by PD0332991 in patients with mantle cell lymphoma. Blood *119*, 4597–4607.

Liu, F., and Korc, M. (2012). Cdk4/6 inhibition induces epithelial-mesenchymal transition and enhances invasiveness in pancreatic cancer cells. Mol. Cancer Ther. *11*, 2138–2148.

Lopez-Mejia, I.C., and Fajas, L. (2015). Cell cycle regulation of mitochondrial function. Curr. Opin. Cell Biol. *33*, 19–25.

Lyssiotis, C.A., Son, J., Cantley, L.C., and Kimmelman, A.C. (2013). Pancreatic cancers rely on a novel glutamine metabolism pathway to maintain redox balance. Cell Cycle *12*, 1987–1988.

Maitra, A., and Hruban, R.H. (2008). Pancreatic cancer. Annu. Rev. Pathol. *3*, 157–188.

Nicolay, B.N., Gameiro, P.A., Tschöp, K., Korenjak, M., Heilmann, A.M., Asara, J.M., Stephanopoulos, G., Iliopoulos, O., and Dyson, N.J. (2013). Loss of RBF1 changes glutamine catabolism. Genes Dev. *27*, 182–196.

Nicolay, B.N., Danielian, P.S., Kottakis, F., Lapek, J.D., Jr., Sanidas, I., Miles, W.O., Dehnad, M., Tschöp, K., Gierut, J.J., Manning, A.L., et al. (2015). Proteomic analysis of pRb loss highlights a signature of decreased mitochondrial oxidative phosphorylation. Genes Dev. *29*, 1875–1889.

Oltersdorf, T., Elmore, S.W., Shoemaker, A.R., Armstrong, R.C., Augeri, D.J., Belli, B.A., Bruncko, M., Deckwerth, T.L., Dinges, J., Hajduk, P.J., et al. (2005). An inhibitor of Bcl-2 family proteins induces regression of solid tumours. Nature *435*, 677–681.

Paulson, A.S., Tran Cao, H.S., Tempero, M.A., and Lowy, A.M. (2013). Therapeutic advances in pancreatic cancer. Gastroenterology *144*, 1316–1326.

Reynolds, M.R., Lane, A.N., Robertson, B., Kemp, S., Liu, Y., Hill, B.G., Dean, D.C., and Clem, B.F. (2014). Control of glutamine metabolism by the tumor suppressor Rb. Oncogene *33*, 556–566.

Roberts, P.J., Bisi, J.E., Strum, J.C., Combest, A.J., Darr, D.B., Usary, J.E., Zamboni, W.C., Wong, K.K., Perou, C.M., and Sharpless, N.E. (2012). Multiple roles of cyclin-dependent kinase 4/6 inhibitors in cancer therapy. J. Natl. Cancer Inst. *104*, 476–487.

Sabharwal, S.S., and Schumacker, P.T. (2014). Mitochondrial ROS in cancer: initiators, amplifiers or an Achilles' heel? Nat. Rev. Cancer *14*, 709–721.

Saif, M.W. (2013). Advancements in the management of pancreatic cancer: 2013. JOP *14*, 112–118.

Sancak, Y., Peterson, T.R., Shaul, Y.D., Lindquist, R.A., Thoreen, C.C., Bar-Peled, L., and Sabatini, D.M. (2008). The Rag GTPases bind raptor and mediate amino acid signaling to mTORC1. Science *320*, 1496–1501.

Serrano, M., Gómez-Lahoz, E., DePinho, R.A., Beach, D., and Bar-Sagi, D. (1995). Inhibition of ras-induced proliferation and cellular transformation by p16INK4. Science *267*, 249–252.

Serrano, M., Lin, A.W., McCurrach, M.E., Beach, D., and Lowe, S.W. (1997). Oncogenic ras provokes premature cell senescence associated with accumulation of p53 and p16INK4a. Cell *88*, 593–602.

Sousa, C.M., and Kimmelman, A.C. (2014). The complex landscape of pancreatic cancer metabolism. Carcinogenesis *35*, 1441–1450.

Thomas, L.W., Lam, C., and Edwards, S.W. (2010). Mcl-1; the molecular regulation of protein function. FEBS Lett. *584*, 2981–2989.

Tibes, R., Qiu, Y., Lu, Y., Hennessy, B., Andreeff, M., Mills, G.B., and Kornblau, S.M. (2006). Reverse phase protein array: validation of a novel proteomic technology and utility for analysis of primary leukemia specimens and hematopoietic stem cells. Mol. Cancer Ther. *5*, 2512–2521.

Vander Heiden, M.G. (2011). Targeting cancer metabolism: a therapeutic window opens. Nat. Rev. Drug Discov. *10*, 671–684.

Váraljai, R., Islam, A.B., Beshiri, M.L., Rehman, J., Lopez-Bigas, N., and Benevolenskaya, E.V. (2015). Increased mitochondrial function downstream from KDM5A histone demethylase rescues differentiation in pRB-deficient cells. Genes Dev. *29*, 1817–1834.

Viale, A., Pettazzoni, P., Lyssiotis, C.A., Ying, H., Sánchez, N., Marchesini, M., Carugo, A., Green, T., Seth, S., Giuliani, V., et al. (2014). Oncogene ablation-resistant pancreatic cancer cells depend on mitochondrial function. Nature *514*, 628–632.

Vincent, A., Herman, J., Schulick, R., Hruban, R.H., and Goggins, M. (2011). Pancreatic cancer. Lancet *378*, 607–620.

Vora, S.R., Juric, D., Kim, N., Mino-Kenudson, M., Huynh, T., Costa, C., Lockerman, E.L., Pollack, S.F., Liu, M., Li, X., et al. (2014). CDK 4/6 inhibitors sensitize PIK3CA mutant breast cancer to PI3K inhibitors. Cancer Cell *26*, 136–149.

Wang, C., Li, Z., Lu, Y., Du, R., Katiyar, S., Yang, J., Fu, M., Leader, J.E., Quong, A., Novikoff, P.M., and Pestell, R.G. (2006). Cyclin D1 repression of nuclear respiratory factor 1 integrates nuclear DNA synthesis and mitochondrial function. Proc. Natl. Acad. Sci. USA *103*, 11567–11572.

Witkiewicz, A.K., Knudsen, K.E., Dicker, A.P., and Knudsen, E.S. (2011). The meaning of p16(ink4a) expression in tumors: functional significance, clinical associations and future developments. Cell Cycle *10*, 2497–2503.

Witkiewicz, A.K., Borja, N.A., Franco, J., Brody, J.R., Yeo, C.J., Mansour, J., Choti, M.A., McCue, P., and Knudsen, E.S. (2015a). Selective impact of CDK4/6 suppression on patient-derived models of pancreatic cancer. Oncotarget *6*, 15788–15801.

Witkiewicz, A.K., McMillan, E.A., Balaji, U., Baek, G., Lin, W.C., Mansour, J., Mollaee, M., Wagner, K.U., Koduru, P., Yopp, A., et al. (2015b). Whole-exome sequencing of pancreatic cancer defines genetic diversity and therapeutic targets. Nat. Commun. *6*, 6744.

Ying, H., Kimmelman, A.C., Lyssiotis, C.A., Hua, S., Chu, G.C., Fletcher-Sananikone, E., Locasale, J.W., Son, J., Zhang, H., Coloff, J.L., et al. (2012). Oncogenic Kras maintains pancreatic tumors through regulation of anabolic glucose metabolism. Cell *149*, 656–670.